Interface contrast imaging for omni-directional full wavefield migration

Hoogerbrugge, L.; Van Dongen, K.; Verschuur, E.

Publication date
2022

Document Version
Final published version

Published in
83rd EAGE Conference and Exhibition 2022

2022 EAGE ANNUAL
83RD CONFERENCE & EXHIBITION
MADRID I SPAIN

INTERFACE CONTRAST IMAGING FOR OMNI-DIRECTIONAL FULL WAVEFIELD MIGRATION

L. Hoogerbrugge[1], K. Van Dongen[1], E. Verschuur[1]

[1] Tu Delft

Summary

Conventional Full Wavefield Migration (FWM) is a full-wavefield inversion method based on recursively applying one-way convolutional propagation and reflection operators in the space-frequency domain at every depth level. Therefore, it struggles to model diving waves and image steep reflectors accurately. In this paper, the Interface Contrast imaging technique, an imaging technique based on the scattering integral developed in the context of medical ultrasound, is presented and used to provide a natural omni-directional extension to the conventional FWM method. The resulting algorithm is applied to a synthetic 2D model featuring a steep reflector. The results of these simulations are given and show that the technique can successfully image steep reflectors. This result yields a proof-of-concept for further research into this algorithm, where including internal scattering is a top priority.

Interface Contrast Imaging for Omni-directional Full Wavefield Migration

Introduction

In recent years, much progress has been made in full wavefield imaging techniques such as Full Waveform Inversion (FWI) (Virieux and Operto, 2009), to obtain high-resolution velocity models, and Full Wavefield Migration (FWM) (Berkhout, 2014b), where all propagation and scattering effects are incorporated in the imaging process. This has led to an increased interest in situations featuring large offsets, which lead to large diving wave amplitudes and allow for the imaging of steep reflectors.

One of the current limitations of FWM is that it is based on one-way propagation between subsequent depth levels, which poses a challenge for imaging diving waves and steep reflectors correctly. Various methods have been proposed to solve these problems. One approach, proposed by Davydenko et al. (2014) and Masaya and Verschuur (2019), is to include horizontal, one-way, propagation and reflection operators in the conventional FWM framework. However, this approach leads to significant cross-talk between horizontal and vertical components of the wave-field and reflectivity. A second approach is to move towards two-way propagation operators by incorporating reverse time migration (RTM) in the FWM framework. This approach has been recently introduced, most notably by Davydenko and Verschuur (2021) and Whitmore et al. (2020). However, this approach leads to higher computational costs, as one must model the wavefield using finite difference methods.

In this abstract, we derive a novel approach to extend the conventional FWM method to the omni-directional case, based on a method called Interface Contrast imaging, developed by van der Neut et al. (2018) in the context of medical ultrasound imaging. This is an omni-directional, integral-based approach, providing a natural extension of FWM to the omni-directional case without significantly increasing computational costs.

Theory

In this section, we derive the forward model of omni-directional FWM. To this end, we consider a spatial domain D_0 with a constant mass density ρ_0, and a spatially varying speed of sound profile $c_0(x)$ and compressibility profile $\kappa_0(x)$. The domain D_0 encloses a spatial sub-domain $D \subset D_0$ with a heterogeneous speed of sound profile $c_1(x)$, mass density profile $\rho_1(x)$ and compressibility profile $\kappa_1(x)$.

The pressure field at a receiver located at a position $\vec{x}_R$ outside D (but inside D_0) can then be found by considering the volume integral formulation of the acoustic scattering problem in the frequency domain, as discussed in van den Berg (2021). This gives

$$P(\vec{x}_R) = P_{inc}(\vec{x}_R) + P_\kappa(\vec{x}_R) + P_\rho(\vec{x}_R), \tag{1}$$

where $P_{inc}(\vec{x}_R)$ is the incident field propagating in D_0 in absence of D, and where the scattered fields $P_\kappa(\vec{x}_R)$ and $P_\rho(\vec{x}_R)$ are defined as:

$$P_\kappa(\vec{x}_R) = -\int_{\vec{x}\in D} \omega^2 \rho_0 G_0(\vec{x}\to\vec{x}_R)\left[\kappa_0(\vec{x}) - \kappa_1(\vec{x})\right] P(\vec{x})\, dV \tag{2}$$

and

$$P_\rho(\vec{x}_R) = \int_{\vec{x}\in D} i\omega \vec{\nabla} G_0(\vec{x}\to\vec{x}_R)\cdot\left[\rho_0 - \rho_1(\vec{x})\right]\vec{V}(\vec{x})\, dV, \tag{3}$$

with ω the angular frequency, $\vec{V}(\vec{x})$ the particle velocity and $G_0(\vec{x}\to\vec{x}_R)$ the Green's function describing the wave propagation in the background medium.

We now examine equation (3) in detail. As the total wavefield is source-free within D, we can write

$$\vec{\nabla} P(\vec{x}) + i\omega\rho_1(\vec{x})\vec{V}(\vec{x}) = 0, \tag{4}$$

for $\vec{x}$ inside D. Using equation (4), we can write equation (3) as

$$P_\rho(\vec{x}_R) = \int_{\vec{x}\in D} \vec{\nabla} G_0(\vec{x}\to\vec{x}_R)\cdot\left(1-\frac{\rho_0}{\rho_1(\vec{x})}\right)\vec{\nabla}P(\vec{x})\,dV. \tag{5}$$

This equation, however, still depends on both $P(\vec{x})$ and $\vec{\nabla}P(\vec{x})$. To eliminate the $\vec{\nabla}P(\vec{x})$ dependence, we use the product rule, hence

$$P_\rho(\vec{x}_R) = \int_{\vec{x}\in D} \vec{\nabla} G_0(\vec{x}\to\vec{x}_R)\cdot\vec{\nabla}\left[\left(1-\tfrac{\rho_0}{\rho_1(\vec{x})}\right)P(\vec{x})\right]dV - \int_{\vec{x}\in D} \vec{\nabla} G_0(\vec{x}\to\vec{x}_R)\cdot P(\vec{x})\,\vec{\nabla}\left(1-\tfrac{\rho_0}{\rho_1(\vec{x})}\right)dV. \tag{6}$$

Using integration by parts, we find

$$P_\rho(\vec{x}_R) = -\int_{\vec{x}\in D} \nabla^2 G_0(\vec{x}\to\vec{x}_R)\left(1-\tfrac{\rho_0}{\rho_1(\vec{x})}\right)P(\vec{x})\,dV + \int_{\vec{x}\in D} \vec{\nabla} G_0(\vec{x}\to\vec{x}_R)\cdot\vec{\nabla}\left(\tfrac{\rho_0}{\rho_1(\vec{x})}\right)P(\vec{x})\,dV. \tag{7}$$

Finally, using the relation $\nabla^2 G_0(\vec{x}\to\vec{x}_R) = -\omega^2 c_0^{-2}(\vec{x})\,G_0(\vec{x}\to\vec{x}_R) - \delta(\vec{x}_R-\vec{x})$, and placing the observation point $\vec{x}_R$ outside D, we find

$$P_\rho(\vec{x}_R) = \int_{\vec{x}\in D} \tfrac{\omega^2}{c_0^2(\vec{x})} G_0(\vec{x}\to\vec{x}_R)\left(1-\tfrac{\rho_0}{\rho_1(\vec{x})}\right)P(\vec{x})\,dV + \int_{\vec{x}\in D} \vec{\nabla} G_0(\vec{x}\to\vec{x}_R)\cdot\vec{\nabla}\left(\tfrac{\rho_0}{\rho_1(\vec{x})}\right)P(\vec{x})\,dV. \tag{8}$$

Combining equation (8) with equations (1) and (2) yields the following expression for $P(\vec{x}_R)$:

$$\begin{aligned} P(\vec{x}_R) = P_{inc}(\vec{x}_R) &- \int_{\vec{x}\in D} \omega^2 G_0(\vec{x}\to\vec{x}_R)\left(\tfrac{1}{c_0^2(\vec{x})}-\tfrac{1}{c_1^2(\vec{x})}\right)\tfrac{\rho_0}{\rho_1(\vec{x})}P(\vec{x})\,dV \\ &+ \int_{\vec{x}\in D} \vec{\nabla} G_0(\vec{x}\to\vec{x}_R)\cdot\vec{\nabla}\left(\tfrac{\rho_0}{\rho_1(\vec{x})}\right)P(\vec{x})\,dV, \end{aligned} \tag{9}$$

with $c_0^{-2}(\vec{x}) = \rho_0\kappa_0(\vec{x})$ and $c_1^{-2}(\vec{x}) = \rho_1(\vec{x})\,\kappa_1(\vec{x})$. Note that we can completely separate the contributions to the scattered fields due to a density contrast and a speed of sound contrast.

We now wish to illustrate how this result can be applied in a seismic context. In order to simplify the analysis, we restrict ourselves to a domain $D\subset D_0$ with a constant density ρ_1 and no contrast in speed of sound with respect to the background, i.e. $c_1(x) = c_0(\vec{x})$. In that case, the scattered $\tilde{P}_\kappa(\vec{x}_R) = 0$ throughout D, and $\tilde{P}_\rho(\vec{x}_R)$ has only non-zero values on the boundary of D, which we denote by ∂D. Consequently, we can write

$$P(\vec{x}_R) = P_{inc}(\vec{x}_R) + \int_{\vec{x}\in\partial D} \vec{\nabla} G_0(\vec{x}\to\vec{x}_R)\cdot\vec{n}(\vec{x})\left(1-\frac{\rho_0}{\rho_1}\right)P(\vec{x})\,dA, \tag{10}$$

with $\vec{n}(\vec{x})$ the (outgoing) normal vector of ∂D. Note that we now only have to integrate over the boundary ∂D of D rather than the whole volume D. We now follow the strategy of van der Neut et al. (2018), and approximate $P(\vec{x})$ as $P(\vec{x})\approx 2\rho_1(\rho_1+\rho_0)^{-1}P_{inc}(\vec{x})$, to reproduce the result of van der Neut et al. (2018):

$$P(\vec{x}_R) = P_{inc}(\vec{x}_R) + 2\int_{\vec{x}\in\partial D}\left(\frac{\partial G_0(\vec{x}\to\vec{x}_R)}{\partial x}Rn_x(\vec{x}) + \frac{\partial G_0(\vec{x}\to\vec{x}_R)}{\partial z}Rn_z(\vec{x})\right)P_{inc}(\vec{x})\,dA. \tag{11}$$

with the reflectivity coefficient R defined as

$$R = \frac{Z_1-Z_0}{Z_1+Z_0} = \frac{\rho_1-\rho_0}{\rho_1+\rho_0}, \tag{12}$$

as the speed of sound $c_0(x)$ is the same for both spatial domains.

Defining $R_x(\vec{x}) = Rn_x(\vec{x})$ and $R_z(\vec{x}) = Rn_z(\vec{x})$, with $R = \sqrt{R_x(\vec{x})^2 + R_z(\vec{x})^2}$, we can now view equation (11) as a forward model to find the wavefield at a receiver given the x and z-components of the reflectivity.

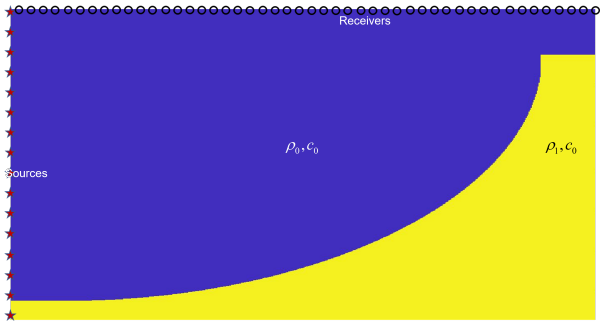

Figure 1 *Model used to generate data. The model has a constant background velocity* $c_0 = 1500$ m/s*, a density* $\rho_0 = 1000$ kg/m^3 *above the reflector and* $\rho_1 = 2500$ kg/m^3 *below the reflector. 16 sources with a spacing of 100 meters, denoted by red crosses, are placed vertically at the left side of the model. 151 receivers with a spacing of 10 meters, denoted by black circles, are located at the top of the model.*

Given a known speed of sound model $c_0(\vec{x})$ and incident wavefield $P_{inc}(\vec{x})$, one can invert this model to find $R_x(\vec{x})$ and $R_z(\vec{x})$, given a known wavefield at the receivers. An example of an inversion result, generated using a gradient descent method, is given in the Results section.

Note that, while equation (11) has been derived in the case of a single reflector and in the absence of speed-of-sound contrasts, it can easily be extended to include increasingly complex geometries. For example, non-zero velocity contrasts can be incorporated by using the definition of the acoustic impedance, $Z = \rho c$. This extension does not take AVO effects into account, but can be used in cases where these can be neglected. Also note that, as the background velocity model $c_0(\vec{x})$ does not need to be constant, propagation effects such as diving waves can be taken into account without loss of accuracy.

Also, multiple reflectors can be taken into account in this framework by iteratively updating the incident wavefield. Using equation (11), one can find the scattered wavefield at the other reflectors. Adding this to the initial incident wavefield allows the method to iteratively update the incoming wavefield and take multiple scattering events into account, following the approach of Berkhout (2014a).

Results

To illustrate the method described in the Theory section, we examine the 2D synthetic model, shown in figure 1. In this model, we examine a highly curved reflector, with a normal that transitions smoothly from 0 degrees to 90 degrees with respect to the z-axis. In order to generate enough illumination on the steep flank of the model, we place the sources vertically in the model and the receivers at the top of the model, simulating a pseudo-borehole situation. Synthetic data is generated using finite difference time-domain modelling. While this model is quite synthetic in its design, it allows us to illustrate the performance for a steep flank case in a homogeneous background.

The results of the inversion process for this model are shown in figure 2. In this figure, four sub-images are shown. In the top-left corner, the true reflectivity model is shown. In the bottom-left corner, the inversion result for the total reflectivity, $R = \sqrt{R_x^2 + R_z^2}$, is shown. Looking at these results, we see that the reflector is well-resolved, both for the horizontal part as for the steep flank. This shows that the method allows us to resolve steep reflectors in the subsurface. Also note the difference between the total reflectivity and its z-component (bottom-right). This difference is relevant, as in conventional FWM one only finds the z-component of the reflectivity (top-right), meaning that the steep part of the reflector will not be resolved using conventional techniques.

Conclusions

In this abstract, we have presented a novel approach to extend the Full Wavefield Migration method to the omni-directional case, using the scattering integral-based Interface Contrast imaging technique.

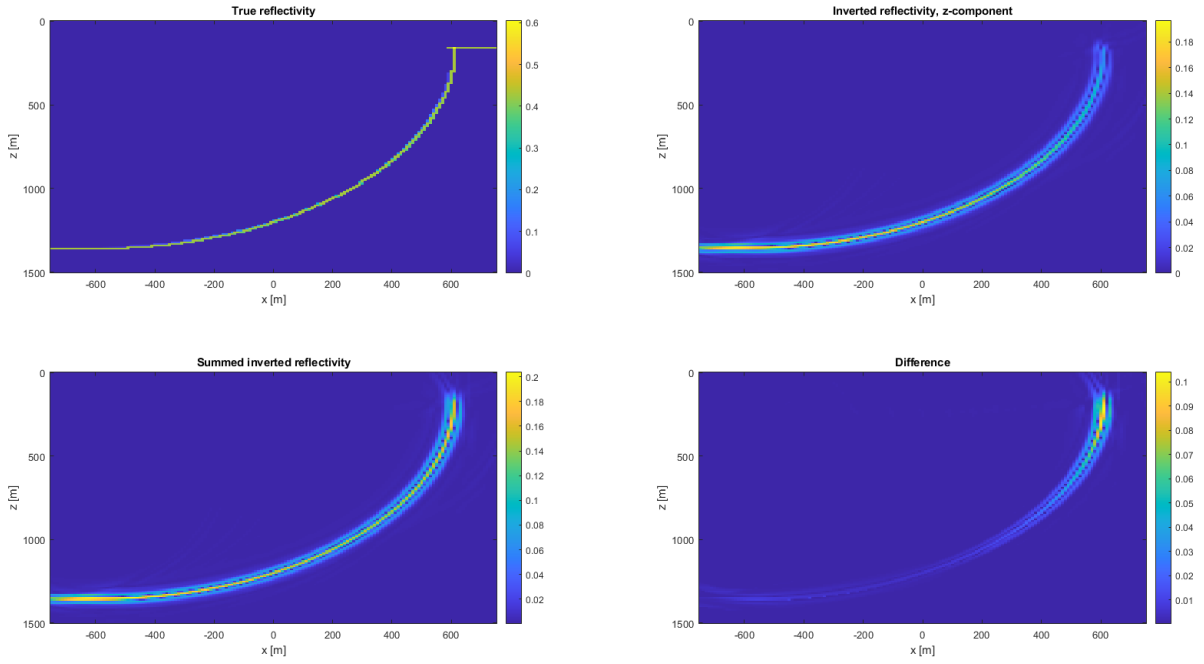

Figure 2 *Result of the inversion process after 10 iterations, showing the true reflectivity (top-left), inverted total reflectivity (bottom-left), inverted z-component (top-right) and difference between the inverted total reflectivity and the inverted z-component (bottom-right).*

Using this technique, we can successfully find reflectors at arbitrary angles, including steep flanks. This technique can be expanded to include more complex geometries, such as models containing strong diving waves or multiple scattering events, and serves as an omni-directional extension to the FWM method.

Acknowledgements

The members of the Delphi consortium are thanked for their support of this research.

References

van den Berg, P.M. [2021] *Forward and Inverse Scattering Algorithms Based on Contrast Source Integral Equations*. Wiley.

Berkhout, A.J. [2014a] Review Paper: An outlook on the future of seismic imaging, Part I: forward and reverse modelling. *Geophysical Prospecting*, **62**, 911–930.

Berkhout, A.J. [2014b] Review Paper: An outlook on the future of seismic imaging, Part II: Full-Wavefield Migration. *Geophysical Prospecting*, **62**, 931–949.

Davydenko, M., Verschuur, D.J. and Berkhout, A.J. [2014] Omnidirectional Extension of Full Wavefield Migration. *Conference Proceedings, 76th EAGE Annual Conference and Exhibition*.

Davydenko, M. and Verschuur, E. [2021] Full wavefield least-squares reverse time migration. *Geophysics*, **86**.

Masaya, S. and Verschuur, D. [2019] Joint Migration Inversion Including Horizontally Propagating Waves. *Conference Proceedings, 81st EAGE Annual Conference and Exhibition*.

van der Neut, J., van den Berg, P.M., Fokkema, J.T. and van Dongen, K.W.A. [2018] Acoustic interface contrast imaging. *Inverse Problems*, **34**.

Virieux, J. and Operto, S. [2009] An overview of full-waveform inversion in exploration geophysics. *Geophysics*, **74**.

Whitmore, N.D., Ramos-Martinez, J., Yang, Y. and Valenciano, A.A. [2020] Seismic modeling with vector reflectivity. *SEG International Exposition and 90th Annual Meeting*.